

Basic circuit compilation techniques for an ion-trap quantum machine

Dmitri Maslov^{1,2}

¹ *National Science Foundation, Arlington, VA, USA*

² *QuICS, University of Maryland, College Park, MD, USA*

dmitri.maslov@gmail.com

May 18, 2022

Abstract

We study the problem of compilation of quantum algorithms into optimized physical-level circuits executable in a quantum information processing (QIP) experiment based on trapped atomic ions. We report a complete strategy: starting with an algorithm in the form of a quantum computer program, we compile it into a high-level logical circuit that goes through multiple stages of decomposition into progressively lower-level circuits until we reach the physical execution-level specification. We skip the fault-tolerance layer, as it is not necessary in this work. The different stages are structured so as to best assist with the overall optimization while taking into account numerous optimization criteria, including minimizing the number of expensive two-qubit gates, minimizing the number of less expensive single-qubit gates, optimizing the runtime, minimizing the overall circuit error, and optimizing classical control sequences. Our approach allows a trade-off between circuit runtime and quantum error, as well as to accommodate future changes in the optimization criteria that may likely arise as a result of the anticipated improvements in the physical-level control of the experiment.

1 Introduction

The interest in quantum computing is rooted in the ability to solve certain computational problems more efficiently by a quantum algorithm than it is known how to do by a regular classical algorithm [15]. To take advantage of those quantum algorithms, a suitable quantum information processing (QIP) system needs to be developed—specifically, one that provides the means to efficiently execute protocols prescribed by the respective quantum algorithms [7]. As of the time of this writing, promising QIP proposals include superconducting [8] and trapped ions [1, 5, 9].

Since the focus of this paper is on the computing over trapped ions QIP platform, we next quickly describe how it works. For details specific to this paper, also see [5]. In the trapped ions QIP the qubits are stored in the spins of the individual ions ($^{171}\text{Yb}^+$ in [5]), with the ions suspended in the free space (vacuum) via the use of magnetic fields. When confined in two dimensions, ions form a line, spanning the remaining spacial dimension. Observed qubit coherence time of $0.5s$ is so long that it is currently not a limiting factor on the size of the computation that is possible to execute; furthermore, it is expected that it can be scaled up by the orders of magnitude in the future [5]. Lasers are used to both initialize the state of the system to a simple state $|00\dots 0\rangle$ via a process called optical pumping, and to read out the state, relying on the fluorescence—specifically, through applying a laser that couples to only one of the two qubit states, and as a result emitting a photon. Both state initialization and measurement are implemented with a very high efficiency—for all practical purposes, that approaching a 100% accuracy. Single- and two-qubit gates are implemented via laser-driven stimulated Raman transitions. This gives rise to the single-qubit physical level gates R and two-qubit XX interaction discussed in detail later in this paper; these gates can

be applied to an arbitrary and selectable set of qubits, and form a computationally universal gate library. Gate fidelities are high, with the demonstrated average CNOT fidelity of 95.6 – 98.5%, depending on the pair of qubits the respective CNOT is being applied to [5]. Note that since the directly implementable elementary gates are R and XX , the CNOT gate itself is a composite transformation. Specifically, [5] uses a 1- XX and 6- R implementation of the CNOT gate¹. The fidelities of the native physical-level R and XX gates are higher than that of the CNOT; we also note that the single-qubit R gates have considerably higher fidelity compared to the XX gates. The authors of [5] furthermore expect to scale physical-level gate fidelities to 99.9% and above with future improvements to the classical control hardware.

Control over systems of several qubits and their interactions has reached a level where quantum algorithms consisting of many dozens of physical gates (*e.g.*, 80 physical single- and two-qubit gates in the QFT5 experiment demonstrated in [5]) are within the reach and circuit optimization becomes a crucial part of their realization. Here we report basic gate decompositions and a general circuit design and optimization approach that can be applied to systematically assemble relevant computational experiments.

We will work with the pure quantum n -qubit states as given by the state vector $\sum_{i=0}^{2^n-1} \alpha_i |i\rangle$ and quantum circuits, defined as the products of quantum gates. A quantum gate over a set of n qubits is described by a $2^n \times 2^n$ unitary matrix U . A square matrix is called unitary iff its complex conjugate equals to its own inverse, $U^{-1} = U^\dagger$. The above formalizes the mathematical properties of the transformations that are possible in principle, but does not specify which of those can be implemented directly on the physical level, or how to compose those physical-level gates into efficient circuit sequences. What is and is not possible to obtain on the physical level furthermore depends on the choice of the QIP platform selected and the controlling apparatus available. In this paper we focus on the trapped ions approach [5]. We first describe physical-level gates obtained in the lab experiment, and show how to use them to efficiently implement known popular logical-level quantum gates such as Pauli gates and their roots, Clifford gates, the CNOT, controlled roots of Paulis, and the Toffoli gate—constituting a set most often used when describing quantum algorithms. Next, we report a generic optimizing compiler mapping logical-level quantum circuits into efficient physical experiments. We conclude the paper with benchmark results showing how the techniques developed can be applied to design optimized quantum computational experiments larger than those demonstrated previously, yet suitable for execution on the existing hardware [5].

2 Single-Qubit Gates

2.1 Physical-level single-qubit rotation

The controlling apparatus allows the application of the single-qubit rotation $R(\theta, \phi)$ described by the following unitary evolution operator:

$$R(\theta, \phi) := \begin{pmatrix} \cos \frac{\theta}{2} & -ie^{-i\phi} \sin \frac{\theta}{2} \\ -ie^{i\phi} \sin \frac{\theta}{2} & \cos \frac{\theta}{2} \end{pmatrix}.$$

Both θ and ϕ can be controlled by changing the duration and phase of the Raman beatnote that drives the Rabi oscillation of the qubit [5].

¹Observe that this paper introduces a 1- XX and 4- R implementation of the CNOT gate, thereby likely improving the CNOT fidelities reported in [5]. The extent to which our optimized implementation improves over the one reported in [5] needs to be established through the experiment.

2.1.1 Single-qubit gate cost

The gate $R(\theta, \phi)$ has two parameters,

$$d := \frac{|\theta|}{\pi} \tau_{1q} \text{ and } e := |\sin(\theta)|\epsilon,$$

where d is the duration of the above single-qubit rotation and e gives a model of the experimental error based on laser pulse area fluctuations due to laser intensity and timing jitter, as suggested in [6]. This leads to random over-/under-rotations of the qubit. The error is proportional to the slope of the Rabi oscillation and hence is smallest for full π rotations [6]. The equipment is currently set up such that it gives the following numeric values for those parameters listed, $\tau_{1q} = 20\mu s$ and $\epsilon \sim 0.01$. Future hardware improvements may reduce the value of ϵ , but unless drastic changes are made to the controlling apparatus, the value τ_{1q} remains the same. As a result, parameter d may be defined as $\frac{20|\theta|}{\pi}\mu s$, whereas parameter e is best defined as a formula over the variable ϵ .

Presently, single-qubit rotations, as well as the two-qubit gates are implemented serially. As a result, the overall runtime of a computational experiment, as described by its circuit, equals to the sum of the runtimes of the individual gates. Depending on the desired properties of the circuit, one may choose to optimize the overall runtime, the overall error, the overall number of gates (including keeping separate counts of the single-qubit and two-qubit gates), as well as any combined figure of the above. In this paper, we will describe the overall cost of an implementation as a length-2 vector (d, e) , with the components corresponding to the overall duration and the overall error. The error component itself is described by the linear combination of all errors from all gates participating in the respective circuit, per the error model introduced for the individual gates. This definition of the error does not correspond to the actual error seen in the experiment, but rather shows the influence and sources of errors within the given implementation. We try to minimize the cost vector (d, e) , focusing separately on the duration and error. One may choose to focus on other optimization criteria, such as, *e.g.*, minimization of the gate count; this does not affect the overall optimization strategy.

For future discussions, we will need the following formulas:

- $R^{-1}(\theta, \phi) = R(\theta, \phi - \pi)$, that can be used to construct the inverse of the $R(\theta, \phi)$ gate at the same cost as the original gate; and
- $R(\theta, \phi) = (-1) \cdot R(\theta - 2\pi, \phi)$, that can be helpful in that it provides the means for limiting the duration of any one $R(\theta, \phi)$ gate to at most $20\mu s$, as the global phase does not matter.

Both identities are easy to verify directly.

2.2 The RX, RY, and RZ rotations

The single-qubit rotations around the basis axes must be expressed in terms of the physical-level R gate to be implementable in an experiment.

RX: Setting $\phi = 0$ in $R(\theta, \phi)$ achieves the rotation about the X axis by the angle θ , as follows:

$$RX(\theta) := \begin{pmatrix} \cos \frac{\theta}{2} & -i \sin \frac{\theta}{2} \\ -i \sin \frac{\theta}{2} & \cos \frac{\theta}{2} \end{pmatrix} = R(\theta, 0). \quad (1)$$

Observe that the duration of $RX(\theta)$ is $\frac{20|\theta|}{\pi}\mu s$, whereas its error is $|\sin \theta|\epsilon$, *i.e.*, its cost vector is $(\frac{20|\theta|}{\pi}\mu s, |\sin \theta|\epsilon)$. The implementation (1) was known to [5].

RY: Setting $\phi = \frac{\pi}{2}$ in $R(\theta, \phi)$ obtains the rotation about Y axis by the angle θ . In particular,

$$RY(\theta) := \begin{pmatrix} \cos \frac{\theta}{2} & -\sin \frac{\theta}{2} \\ \sin \frac{\theta}{2} & \cos \frac{\theta}{2} \end{pmatrix} = R(\theta, \pi/2). \quad (2)$$

As a result, the cost of $RY(\theta)$ is $\left(\frac{20|\theta|}{\pi} \mu s, |\sin \theta| \epsilon\right)$. The implementation (2) was also known to [5]. The costs of the RX and RY gates with the same rotation angle are thus the same. RZ is more difficult to obtain. In particular,

RZ: RZ rotation is defined as follows,

$$RZ(\theta) := \begin{pmatrix} e^{-i\theta/2} & 0 \\ 0 & e^{i\theta/2} \end{pmatrix}.$$

It is not difficult to show that it cannot be obtained via a single physical R pulse, and thus requires a circuit with two or more R gates. Firstly, we found the following circuit implementing the RZ gate

$$\begin{aligned} RZ(\theta) &= RY \left((-1)^{b+1} \frac{\pi}{2} \right) . RX \left((-1)^b \theta \right) . RY \left((-1)^b \frac{\pi}{2} \right) \\ &= R \left((-1)^{b+1} \frac{\pi}{2}, \frac{\pi}{2} \right) . R \left((-1)^b \theta, 0 \right) . R \left((-1)^b \frac{\pi}{2}, \frac{\pi}{2} \right), \end{aligned} \quad (3)$$

where b is a Boolean variable allowing to arbitrarily set the sign of either first or last RY rotation, and ‘.’ denotes matrix multiplication (recall that the order of gates in the circuit is given by the inverted order of matrices in the matrix product). The implementation with $b = 0$ was known to [5]; as we will show later, the ability to choose the sign of b , being our contribution to the above circuit, is very important in circuit optimization. The cost of this implementation is $\left(\frac{20|\theta|}{\pi} + 20 \mu s, 2 \times \epsilon + 1 \times |\sin \theta| \epsilon\right)$. Alternatively, $RZ(\theta)$ gate may be obtained as

$$RZ(\theta) \equiv R(\pi, x) . R(\pi, x - \theta/2), \quad (4)$$

up to an undetectable global phase of -1 (equality up to a global phase is furthermore denoted by ‘ \equiv ’), where the parameter x may be set arbitrarily. The cost of this implementation is $(40 \mu s, 2 \times |\sin \pi| \epsilon) = (40 \mu s, 0)$. Observe that with the slightly longer execution time this second realization is associated with a much smaller error, which seems to be a preferred scenario in the physical experiments. The flexibility in setting x within the above implementation allows to optimize quantum circuits where RZ is one of the gates used, as varying the value x allows to obtain either the $RX(\pi)$ gate or the $RY(\pi)$ gate to be either first or last gate in (4), and those may cancel out with other gates in the circuit. Varying parameter x furthermore allows optimizing classical control, as selecting a value of the R gate parameter used to implement a previous single-qubit gate allows to keep the phase of the Raman beatnote used a constant. This, however, is only a minor improvement to the classical control sequences. Implementation (3) may become more desirable for the purpose of circuit optimization, since it relies on the efficiently optimizable sequence of RX and RY gates.

$RX(\pi)$, $RY(\pi)$, and $RZ(\pi)$ implement Pauli-X, Pauli-Y, and Pauli-Z gates up to an undetectable global phase of $-i$. $RX(\pi/2)$ implements the square-root-of-NOT gate $V := \frac{1+i}{2} \begin{pmatrix} 1 & -i \\ -i & 1 \end{pmatrix}$ up to a global phase. The rotation $RZ(\pi/2)$ implements the quantum Phase gate (commonly referred to as P or S) $P := \begin{pmatrix} 1 & 0 \\ 0 & i \end{pmatrix}$ up to a global phase. The quantum $\pi/8$ gate also known as the T gate, $T := \begin{pmatrix} 1 & 0 \\ 0 & \frac{1+i}{\sqrt{2}} \end{pmatrix}$, is obtained as $RZ(\pi/4)$, up to a global phase.

Recall that RX , RY , and RZ gates do not commute, but their parameters may be added, *i.e.*, $G(a)G(b) = G(a+b)$, when G is either one of RX , RY , or RZ . This is important for the circuit optimization technique discussed later.

2.3 Other common single-qubit rotations

A common single-qubit gate that may not be expressed as an axial rotation with a certain parameter is the Hadamard gate, $H := \frac{1}{\sqrt{2}} \begin{pmatrix} 1 & 1 \\ 1 & -1 \end{pmatrix}$. It can be implemented up to a global phase as one of the following two circuits.

$$\begin{aligned} H &\equiv RY(-\pi/2).RX(\pi) = R(\pi/2, \pi/2).R(\pi, 0), \\ H &\equiv RX(-\pi).RY(\pi/2) = R(-\pi, 0).R(\pi/2, \pi/2). \end{aligned}$$

The cost of each of the above circuits is $(30\mu s, \epsilon)$. As such, the Hadamard gate is, roughly speaking, as expensive as the RZ rotation, and more expensive than either RX or RY . The ability to choose which of the RX/RY gates in the decomposition of the Hadamard gate comes first and which is second is important to the optimization of quantum circuits.

2.4 Arbitrary single-qubit rotations

An arbitrary single-qubit unitary gate can be written as a matrix $U = e^{id} \begin{pmatrix} e^{ia} \cos b & e^{ic} \sin b \\ -e^{-ic} \sin b & e^{-ia} \cos b \end{pmatrix}$ of four real-valued parameters a, b, c , and d . We found the following implementation as a circuit with at most two physical-level R gates,

$$U \equiv \begin{pmatrix} e^{ia} \cos b & e^{ic} \sin b \\ -e^{-ic} \sin b & e^{-ia} \cos b \end{pmatrix} = R(-\pi, -c - \pi/2).R(2b + \pi, a - c - \pi/2). \quad (5)$$

The cost of this implementation is $(20 + \frac{20|2b \bmod \pi|}{\pi} \mu s, |\sin(2b)|\epsilon)$. Observe, that equation (5) uses the minimal number of physical-level gates R required to implement an arbitrary single-qubit unitary. This can be established by counting the number of the real-valued degrees of freedom in the 2×2 unitary matrices up to the global phase, and comparing it to the number of the real-valued degrees of freedom of the R gates. Equation (5) furthermore gives rise to the following Lemma providing a guarantee on the cost of quantum physical-level circuits.

Lemma 1. Any quantum physical-level circuit over n qubits with G two-qubit XX gates can be reduced to an equivalent one with no more than $2(n + 2G)$ single-qubit R gates, providing, across all single-qubit gates used, an overall contribution of no more than $40(n + 2G)\mu s$ to the runtime and a term of no more than $(n + 2G) \times \epsilon$ to the error.

Proof: First, count the number of the “pieces of wire”, defined as an uninterrupted by any two-qubit gate qubit evolution time piece between two two-qubit gates in the circuit. This number is given by the expression $n + 2G$, as is easy to verify by induction on G , the number of the two-qubit gates. Indeed, there are n pieces of wire in quantum circuits with no two-qubit gates, and the introduction of a two-qubit gate at the end of the circuit increases the number of the pieces of wire by two (specifically, on those qubits that the given two-qubit gate operates on). The single-qubit operations are contained to the individual pieces of wire, allowing to conclude the proof by referring to the equation (5) and the definitions of the duration and error. \square

The above Lemma reports an upper bound on the number of single-qubit gates, and could be used as a bottom line comparison for evaluating the efficiency of the optimizing compiler developed and tested in Sections 4-5. We furthermore observe that the above Lemma applies to show that the 5-qubit 80-gate QFT5 circuit, of which 10 are two-qubit gates reported in [5] is suboptimal. This is because according to Lemma 1 the upper bound on the number of gates in such a circuit is 60.

3 Two-Qubit Gates

3.1 Physical-level two-qubit gate

The physical-level two-qubit gate available to us is the so-called $XX(\chi)$ gate, with parameter χ that depends on the pair of ions the gate is being applied to. The gate itself is defined by the following unitary matrix [5]:

$$XX(\chi) = \begin{pmatrix} \cos(\chi) & 0 & 0 & -i \sin(\chi) \\ 0 & \cos(\chi) & -i \sin(\chi) & 0 \\ 0 & -i \sin(\chi) & \cos(\chi) & 0 \\ -i \sin(\chi) & 0 & 0 & \cos(\chi) \end{pmatrix}$$

The absolute value of the phase, $|\chi|$, can be set to any arbitrary real number by varying the laser power used in the experiment [5]. The sign of χ depends on the laser detuning which is chosen based on the normal modes a particular pair of ions interacts with most strongly and hence which qubits the gate is being applied to [5]. The sign for each two-qubit gate is thus fixed experimentally and becomes an input parameter for how one is allowed to construct circuits.

The $XX(\chi)$ gate implements the well-known Mølmer-Sørensen gate [19], and latter is known to generate the CNOT gate (in the case of XX gates for $\chi = \pm\pi/4$) using single-qubit operations on the input and the output side. The CNOT gate is an important computational primitive—the ability to obtain it, coupled with the ability to implement any single-qubit gate, see equation (5), gives computational universality [2]. However, the ability to vary parameter χ to accept values beyond $\pm\pi/4$ allows a more efficient implementation of important quantum gates. Once computational universality is obtained, the efficiency becomes a next important step.

The following property of the $XX(\chi)$ gate is important to note for future discussions: $XX(\chi)$ commutes with any single-qubit $RX(\theta)$ rotation. However, $XX(\chi)$ does not commute with either $RY(\theta)$ or $RZ(\theta)$ when $\theta \not\equiv 0 \pmod{2\pi}$.

3.1.1 Cost function variables

The two-qubit $XX(\chi)$ gate has the vector-function cost (d, e) , where [6]:

$$d := 235\mu s \text{ and } e := |\sin(2\chi)|E.$$

Here, d is the duration of the two-qubit XX rotation, and e is the error due to fluctuations in the experiment, analogous to the single-qubit case. Usually, $E \sim 0.04$, but its value may vary slightly depending on the set of qubits the gate is being applied to. In the current experimental setup [5], the two-qubit gates XX cannot be applied in parallel, however, an XX gate can be applied to any pair of qubits.

Compared to the single-qubit gate R , the two-qubit gate is substantially longer in runtime and has a higher error. As a result, efficient circuit implementations must prefer the minimization of the use of the two-qubit XX gate over minimizing the single-qubit gates.

3.2 Constructing the CNOT gate

Depending on the sign of χ for the given set of qubits that we want to apply the CNOT gate to, it can be implemented up to a global phase as one of the two circuits, such as shown in Figure 1. Observe that b is a Boolean variable that may be chosen arbitrarily to set the signs of the parameter in RY at the beginning or at the end of those implementations. In particular, parameter b may be chosen such as to

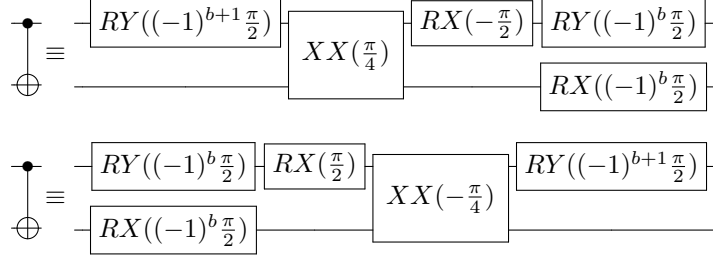


Figure 1: Implementation of the CNOT gate using physical-level gates.

set the value of the first RY rotation to the positive number, $+\frac{\pi}{2}$, in which case the second RY features the negative sign, or vice versa. The ability to choose the sign is particularly important in allowing single-qubit RY gate cancellations while decomposing logical-level circuits with multiple CNOT gates into efficient physical-level circuits.

The cost of the above implementations of the CNOT gate is $(275\mu s, 1 \times E + 4 \times \epsilon)$.

Other than using two fewer single-qubit gate pulses compared to [20], our CNOT implementation allows to arbitrarily set the values of the RY rotations, and also allows further transformations and optimizations per template (7) discussed later. Our CNOT implementation saves two single-qubit pulses (one $RX(\pm\frac{\pi}{2})$ and one $RY(\pm\frac{\pi}{2})$) over the one reported in [5].

3.3 Constructing controlled-roots of Paulis

Controlled roots of axial rotations (Pauli gates) play an important role in quantum circuits. For instance, the n -qubit quantum Fourier transform is best viewed as a circuit with $\frac{n(n-1)}{2}$ controlled roots of Pauli- Z gates [15, Figure 5.1]. The controlled-sqrt-NOT gate is used in the construction of an efficient five two-qubit gate circuit implementing the Toffoli gate [2, Lemma 6.1]. Otherwise, if the proper root is not available, and the CNOT gate is the only two-qubit gate directly constructible, the Toffoli gate requires six two-qubit physical gates [18]. It is furthermore known that each controlled unitary gate can be implemented with the use of two CNOT gates, and, equivalently, two Mølmer-Sørensen gates, along with some single-qubit gates [2, Lemma 5.1]. We next show that only one $XX(\chi)$ gate suffices to implement any controlled root of a Pauli gate, providing an improvement by a factor of two. In particular, depending on the sign of χ , the controlled- X^α , $\alpha \in \mathbb{R}$, $-1 \leq \alpha \leq 1$, may be obtained as follows:

$$\begin{aligned}
 & \begin{array}{c} \text{---} \bullet \text{---} \\ | \\ \text{---} X^\alpha \text{---} \end{array} \equiv \begin{array}{c} \text{---} RY(-\frac{\pi}{2}) \text{---} \\ | \\ \text{---} XX(\frac{\alpha\pi}{4}) \text{---} \\ | \\ \text{---} RX(\frac{\alpha\pi}{2}) \text{---} \end{array} \begin{array}{c} \text{---} RX(-\frac{\alpha\pi}{2}) \text{---} RY(\frac{\pi}{2}) \text{---} \\ | \\ \text{---} RX(\frac{\alpha\pi}{2}) \text{---} \\ | \\ \text{---} RY(-\frac{\pi}{2}) \text{---} \end{array} \quad (6) \\
 & \begin{array}{c} \text{---} \bullet \text{---} \\ | \\ \text{---} X^\alpha \text{---} \end{array} \equiv \begin{array}{c} \text{---} RY(\frac{\pi}{2}) \text{---} RX(\frac{\alpha\pi}{2}) \text{---} \\ | \\ \text{---} XX(-\frac{\alpha\pi}{4}) \text{---} \\ | \\ \text{---} RX(\frac{\alpha\pi}{2}) \text{---} \end{array} \begin{array}{c} \text{---} RY(\frac{\pi}{2}) \text{---} \\ | \\ \text{---} RY(-\frac{\pi}{2}) \text{---} \end{array}
 \end{aligned}$$

The inverse of the controlled- X^α may be obtained from the above formulas by attempting to construct the controlled- $X^{-\alpha}$. Observe that the decomposition with the sign opposite to the physically available sign of χ needs to be selected. Other controlled roots of Paulis, such as controlled- Y^α and controlled- Z^α are related to the controlled roots of the NOT gate by the following formulas,

$$\begin{aligned}
 & \begin{array}{c} \text{---} \bullet \text{---} \\ | \\ \text{---} Y^\alpha \text{---} \end{array} = \begin{array}{c} \text{---} \bullet \text{---} \\ | \\ \text{---} P^\dagger \text{---} X^\alpha \text{---} P \text{---} \end{array} \\
 & \begin{array}{c} \text{---} \bullet \text{---} \\ | \\ \text{---} Z^\alpha \text{---} \end{array} = \begin{array}{c} \text{---} \bullet \text{---} \\ | \\ \text{---} H \text{---} X^\alpha \text{---} H \text{---} \end{array}
 \end{aligned}$$

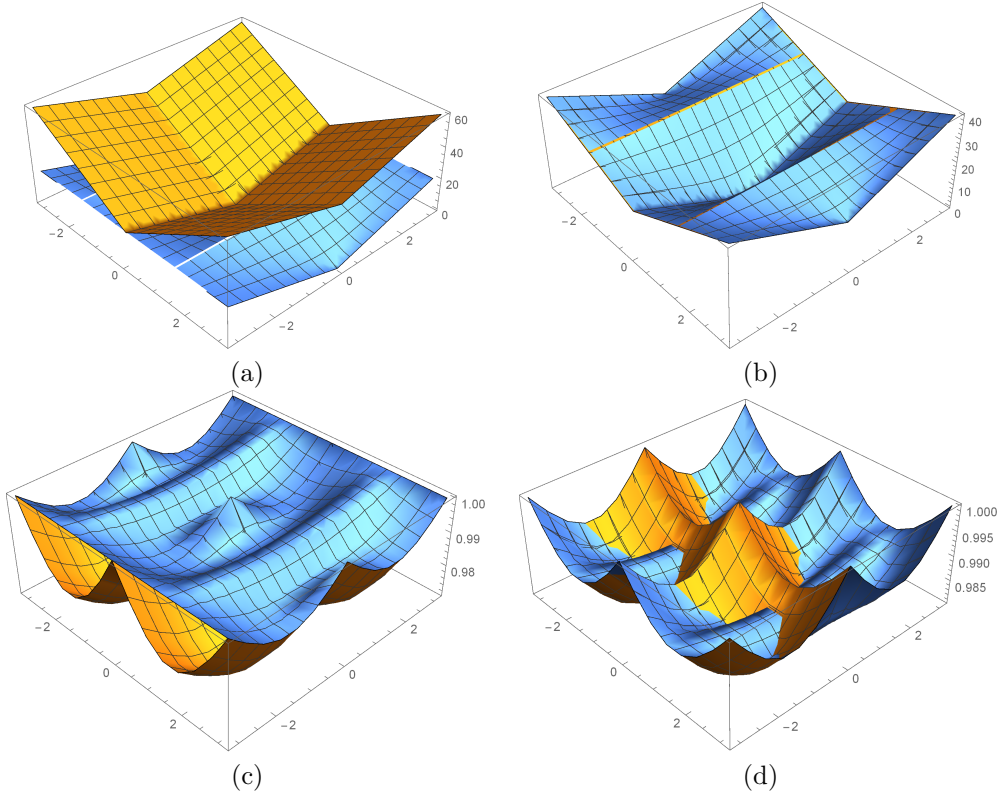


Figure 2: (a) change in the duration (old: yellow, new:blue; lower is better) in replacing $RX(a)RY(b)RX(a)$, $a, b \in [-\pi, \pi]$ by $R(c, d)$ measured in μs ; (b) change in the duration (old: yellow, new:blue; lower is better) in replacing $RX(a)RY(b)$, $a, b \in [-\pi, \pi]$ by $R(c, d)RX(-a)$ measured in μs ; (c) change in the fidelity (old: yellow, new: blue; higher is better) in replacing $RX(a)RY(b)RX(a)$, $a, b \in [-\pi, \pi]$ by $R(c, d)$ for $\epsilon = 0.01$; (d) change in the fidelity (old: yellow, new: blue; higher is better) in replacing $RX(a)RY(b)$, $a, b \in [-\pi, \pi]$ by $R(c, d)RX(-a)$ for $\epsilon = 0.01$. Fidelity of the circuit spanning a single qubit with the gates G_1, G_2, \dots, G_k featuring the individual errors e_1, e_2, \dots, e_k is calculated as the product $\prod_{i=1}^k (1 - e_i)$. This corresponds to the model where the errors are independent, and is consistent with the understanding of the physics and source of errors in the R gates [5, 6].

As a result, all controlled roots of Paulis are constructible using at most one physical-level two-qubit XX gate.

3.4 Useful single-qubit circuit identity

Recall that a quantum template is a quantum circuit with n gates that evaluates to the identity, $G_0 G_1 \dots G_{n-1} = Id$ [12]. A template can be used to construct a number of circuit identities,

$$G_i G_{i+1 \bmod n} \dots G_{i+k-1 \bmod n} = G_{i-1 \bmod n}^{-1} G_{i-2 \bmod n}^{-1} \dots G_{i+k \bmod n}^{-1},$$

for arbitrary i and k , $0 \leq i, k \leq n$, which may, in turn, be used to optimize quantum circuits via matching gates on the left hand side in the above equation and replacing them with the gates on the right hand side. Here we report one such template that is particularly useful in our constructions. Specifically, for any $a, b \in \mathbb{R}$ there exist $c, d \in \mathbb{R}$ such that:

$$\boxed{RX(a)} \boxed{RY(b)} \boxed{RX(a)} \boxed{R(c, d - \pi)} = \text{---} \quad (7)$$

$$\text{where} \quad c := 2 \arccos \left(\cos a \cdot \cos \frac{b}{2} \right),$$

$$d := \begin{cases} \arcsin \left(\frac{\sin \frac{b}{2}}{\sqrt{1 - \cos^2 a \cdot \cos^2 \frac{b}{2}}} \right) & \text{if } a > 0 \\ \pi - \arcsin \left(\frac{\sin \frac{b}{2}}{\sqrt{1 - \cos^2 a \cdot \cos^2 \frac{b}{2}}} \right) & \text{if } a < 0. \end{cases}$$

The above template may be used in multiple ways.

- Firstly, it allows the replacement of $RX(a)RY(b)RX(a)$ with $R(c,d)$. The latter circuit always has a smaller duration and a higher overall fidelity (smaller contribution to the overall error), see Figure 2(a)(c).
- This template may be used to replace $RX(a)RY(b)$ with $R(c,d)RX(-a)$ and $RY(b)RX(a)$ with $RY(b)RX(-a)R(c,d)$. This allows to trade off runtime for error, see Figure 2(b)(d) for the illustration of the changes in the runtime and error. While the runtime always increases, it is sometimes possible to improve the fidelity. For instance, if $RX(\frac{\pi}{2})RY(-\frac{\pi}{2})$ in the circuit in Figure 1 were replaced with $R(\pi, -\frac{\pi}{4})RX(-\frac{\pi}{2})$ this would result in the cost vector change of that part of the computation from $(20\mu s, 2 \times \epsilon)$ to $(30\mu s, \epsilon)$. This constitutes an increase of the runtime by $10\mu s$ over the increase of the fidelity by the additive term $\epsilon - \epsilon^2$. Since the above rule applies to any pair RX and RY , it allows substantial flexibility in exchanging runtime for error.

4 Compiling quantum algorithms into physical-level circuits

Define two circuit cost metrics, a coarse-grain and a fine-grain one. The coarse-grain metric counts the number of the two-qubit controlled roots of Paulis in quantum circuits. The fine-grain metric is described by the cost vector $(time, error)$, where *time* sums up the runtimes across all gates used, and *error* combines all errors. Note that once the controlling apparatus allowing to execute gates in parallel is developed, the definition of *time* will change into the sum of times across the critical path; other changes to the above costing metrics may also be accommodated, and depend on the improvements in the controlling apparatus.

The following reports all steps taken by our overall design approach that maps a quantum algorithm into an optimized physical-level experiment.

1. Choose an algorithm and map it into a high-level logical circuit with the help of a quantum programming language, if needed.
2. Synthesize all arithmetic and oracle parts, if not explicitly supplied. Arithmetic circuits are chosen from the known libraries, and oracles are synthesized using known reversible logic synthesis algorithms [17]. Optimize the resulting implementation over the coarse-grain cost metric [11].
3. Decompose the multiple-control Toffoli gates into smaller gates, such as three-qubit Toffoli gate and small relative phase Toffoli gates [10]. Optimize circuits using peep-hole [16] and templates [12] over the coarse-grain cost metric.
4. Break down all gates into two-qubit controlled roots of Paulis and arbitrary single-qubit gates using optimal implementations [15], and optimize the resulting decompositions using templates [12] over the coarse-grain metric. At the end of this stage we should have reached the limit of optimization of the number of most expensive two-qubit gates, therefore we will next switch the gear and employ the fine-grain metric.
5. Map logical qubits into physical qubits such as to minimize the use of the least desired interactions (those associated with the least two-qubit XX gate fidelities), and maximize gate cancellations during further optimization. To accomplish latter, record the position and the signs of all $RY(\pm\frac{\pi}{2})$

gates participating in the expansions of the powers of controlled roots of Paulis that cannot be varied but depend of the sign of χ (6), and favour the selection of physical qubit mapping resulting in R_Y cancellations on the control qubit. The cancellation happens between two controls when there are no gates between them, and the signs of χ corresponding to the two XX rotations are equal. In general, so long as the number of the qubits remains small, this can be done exhaustively; otherwise, a mix of subgraph isomorphism and greedy heuristics can be employed.

6. Decompose further into physical-level circuit and optimize the resulting implementation:
 - (a) Perform controlled root of Pauli gate substitutions—those are now uniquely defined per formulas (6). Choose CNOT, H , and RZ gate decompositions such as to maximize the cancellations of pairs $R_Y(\pm\frac{\pi}{2})$ and $R_Y(\mp\frac{\pi}{2})$. Perform CNOT, H , and RZ gate substitutions as circuits over XX , RX , R_Y , and R gates favouring the heavy use of the RX and R_Y , and then reduce the number of RX and R_Y gates.
 - (b) Perform substitution of all other gates, favouring the use of RX and R_Y gates. Perform cancellations by commuting RX gates past XX gates, and adding parameters of the same type neighbouring gates. Use template (7) to optimize sequences $RX - R_Y - RX$. This operation can be done via considering a single qubit in a circuit at a time, and commuting RX all the way to the selected R_Y .
 - (c) Perform balancing of runtime vs error using template (7) until the desired balance is found or no more improvement can be achieved. If the single-qubit gate sequences of length 3 and higher are found, replace them with 2 R gates sequences, per formula (5).
 - (d) Rewrite all remaining single-qubit RX and R_Y gates as the physical-level R pulses.

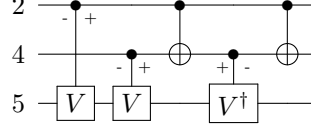
The bulk of work and the optimization not previously considered in the literature falls into steps 5 and 6 of the above approach. The complexity of the algorithms employed in step 6 is described by a low degree polynomial in the number of gates in the circuit (the degree of the polynomial depends on the details of the template application algorithm, and with some restrictions can be as small as linear). The complexity of the algorithms used in step 5 depends on the efficiency of subgraph isomorphism or other heuristics employed. Steps 1-4 rely on a combination and a modification of the known techniques.

5 Benchmark results

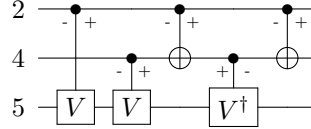
The physical trapped ions machine we have access to [5] has the following signs of χ , depending on the specific interactions used: χ has a positive sign for interactions 12, 14, 23, 25, 34, 35, and 45. The sign is negative for the interactions 13, 15, and 24. Due to the values of physical errors, we expect to be able to apply circuits containing no more than about 15 two-qubit gates, therefore the bulk of work in this section is devoted to developing and optimizing experiments that satisfy the above condition. Specifically, our goal in this section is to propose experiments maximally utilizing the capabilities of the trapped ions machine [5], as well as to design those experiments with maximal efficiency and in a systematic way. In the coming subsection we illustrate how the above circuit compilation techniques accomplish the task of implementing the Boolean multiplication, and then report the results of the design of advanced experiments. Majority of the advanced experiments proposed here scale beyond those computations previously demonstrated in an experiment.

A somewhat relevant work on the circuit optimization for trapped ions technology was performed in [14], that relied on the use gradient ascend type algorithm to optimize the gate sequences. Our optimization is based on establishing the relation between gate decompositions, and applying the template (7), and therefore we expect the computational complexity as well as the practical efficiency of our algorithms to be better compared to the gradient-ascend type techniques. Indeed, our approach is so simple that, unlike [14], we did not yet need to resort to a computer search. While

- a. Now that the signs of $\chi_{i,j}$ are known, mark controls of the controlled- V gates with $+/-$ by the sign of the RY rotation that appears on it when decomposed into physical pulses using formulas (6),



and then choose the CNOT gate decompositions (Figure 1) such as to maximize RY cancellations,



The above choice for the CNOT decompositions allows to cancel two pairs of $RY(\frac{\pi}{2})/RY(-\frac{\pi}{2})$ gates on the first qubit, as evidenced by the “meeting” plus and minus signs.

- b. Perform gate substitutions and cancellations to obtain the circuit shown in Figure 3(a).
- c. The rest of the single-qubit optimization algorithm is based on the template (7), and works differently depending on the criteria for the remaining optimization. If the runtime is the goal, the algorithm tries to find triples of gates $RX - RY - RX$ that may be replaced with the R gate, such as to minimize the overall duration. This allows to construct the circuit pictured in Figure 3(b). In case if minimizing the error is preferred, the algorithm tries to find suitable pairs RX/RY that can be replaced with a pair of R and RX gate featuring a smaller error. The result of this optimization may be found in Figure 3(c). We conclude the optimization by layering the single-qubit gates sharing the same duration, by moving RX , whenever possible, such as to allow their sequential execution—this helps to optimize classical controlling sequences.

Observe that at the stage of the decomposition of the two-qubit logical gates into implementable physical-level gates, the single-qubit pulse count was 20. The parametrized CNOT implementation per Figure 1, along with the algorithm for joint gate decomposition, and RX gates commutation over the application of template (7) allowed to reduce the single-qubit pulse count from the original 20 down to 9 (Figure 3(c)). Had the previously known circuitry implementing the CNOT gate with two more single-qubit pulses [5, 20] been used, the original unoptimized single-qubit gate count would have been 30. The upper bound on the number of single-qubit gates in a circuit of this size, as given by the application of Lemma 1, is 26. Had the efficient controlled-root-of-Pauli implementation introduced in this paper been not used, the resource count would have been substantially higher—not only the single-qubit gates, but this time, two-qubit gates as well. This illustrates the power of the approach reported in this paper.

Our Toffoli gate implementation, Figure 3(b) takes time 1275 μs , which compares favourably to 1500 μs reported in [13]. The advantage in the duration, however, is attributed to the more advanced hardware [5] that we rely on in our work. The major difference between our implementation and the one reported in [13] is our circuit is a true Toffoli gate that can be used (and in fact is used in the next subsection) as a primitive in the implementation of quantum algorithms, whereas [13] reports a Toffoli gate implemented up to a relative phase; such an implementation up to the relative phase may not be used in quantum algorithms—specifically, it would give an incorrect answer if used within Grover’s search [4].

5.2 Advanced experiments

Table 1 reports the result of the application of the above techniques to the design and optimization of circuits implementing advanced quantum computational experiments. None of the implementations proposed in Table 1 have yet been demonstrated in an experiment. Table 1 lists the name of the

Function	#q	1q/2qg	Time	Error
Grover ^{011,111}	4	29/10	2743 μs	$6 \times 0.707107\epsilon + 4 \times 0.866025\epsilon + 9 \times \epsilon + 6 \times 0.707107E + 4 \times E$
Grover ^{011,101}	4	31/12	3250 μs	$6 \times 0.707107\epsilon + 3 \times 0.866025\epsilon + 10 \times \epsilon + 6 \times 0.707107E + 6 \times E$
Grover ^{010,100}	4	32/12	3280 μs	$6 \times 0.707107\epsilon + 3 \times 0.866025\epsilon + 10 \times \epsilon + 6 \times 0.707107E + 6 \times E$
Grover ^{000,111}	4	31/13	3492 μs	$4 \times 0.707107\epsilon + 5 \times 0.866025\epsilon + 10 \times \epsilon + 6 \times 0.707107E + 7 \times E$
QFT4	4	13/6	1582 μs	$1 \times 0.273262\epsilon + 1 \times 0.382683\epsilon + 2 \times 0.521005\epsilon + 1 \times 0.866025\epsilon + 1 \times 0.92388\epsilon$ $+ 2 \times 0.980785\epsilon + 4 \times \epsilon + 1 \times 0.19509E + 2 \times 0.382683E + 3 \times 0.707107E$
QFT5	5	22/10	2669 μs	$1 \times 0.138284\epsilon + 1 \times 0.273262\epsilon + 1 \times 0.521005\epsilon + 1 \times 0.55557\epsilon + 1 \times 0.707107\epsilon$ $+ 1 \times 0.722528\epsilon + 1 \times 0.831147\epsilon + 2 \times 0.866025\epsilon + 1 \times 0.951173\epsilon + 2 \times 0.995185\epsilon$ $+ 4 \times \epsilon + 1 \times 0.098017E + 2 \times 0.19509E + 3 \times 0.382683E + 4 \times 0.707107E$
Toffoli-4	5	21/11	2832 μs	$8 \times 0.707107\epsilon + 2 \times 0.866025\epsilon + 4 \times \epsilon + 3 \times 0.707107E + 8 \times E$

Table 1: Benchmark circuits.

algorithm/function, the number of qubits the developed implementation uses, the number of physical-level single-qubit/two-qubit pulses, the overall runtime of the circuit, and all sources of errors. All implementations reported in Table 1 are true implementations of the respective algorithms/functions, in that we report exact unitaries (VS those up to relative phase), treat black boxes as black boxes (no optimizations crossing black box boundaries), as well as precisely follow the formulation of the respective algorithms and specifications. Our computations are thus properly scalable to accept larger numbers of qubits. The quantum state is furthermore initialized to $|00000\rangle$ (as opposed to a state containing partial results of a computation) before any of the circuits are applied.

For Grover’s algorithm, we considered the scenario when the three-bit Boolean function $f(x) = f(x_1, x_2, x_3)$ implemented as Grover’s oracle, $|x, y\rangle \mapsto |x, y \oplus f(x)\rangle$, marks some two items in the database. There are 28 such functions. The superscript in the name of the Grover’s function in Table 1 indicates the bit strings encoded by the oracle the search over which is being reported. The efficiency of the Grover’s circuit is determined by the efficiency of the implementation of the oracle, which in turn is determined by the Hamming distance between those items it marks. We treat the oracle as a black box, and do not allow optimizations across the boundary of the black box. While we can implement Grover’s algorithm over any oracle marking two items, only a few representative circuits are actually included in the Table. To implement Grover’s algorithm over a Boolean function marking one item, the oracle needs to be a Toffoli-4 gate (the triply-controlled Toffoli, $\text{TOF}[a, b, c; d]$). We calculated that the single Grover’s iteration requires 16 two-qubit gates. The algorithmic probability of reading out the correct answer upon applying a single Grover’s iterate is 0.78125, which beats the classical probability of finding the answer with the single query, 0.125, therefore, it may be interesting to run such an experiment, as well.

The QFT5 circuit reported in Table 1 can be compared head-to-head to the one found in [5]. Specifically, both circuits are true [15, Figure 5.1] (as opposed to semiclassical, [3]) implementations of the 5-qubit QFT, featuring 10 two-qubit gates. Our circuit benefited from careful design, and as a result features the single-qubit gate count of just 22 compared to 70 in [5]. This constitutes the reduction of the single-qubit gate count by a factor of more than three, clearly illustrating the benefits of our approach.

To our knowledge, the Toffoli-4 gate circuit reported in Table 1 is the first such containing no more than 11 two-qubit gates. Previous best result is 12 CNOTs [10].

6 Conclusion

In this paper we reported a complete strategy for automatic execution of quantum algorithms on a trapped ions quantum machine. Our contributions include the design of the complete data flow from the algorithm level down to the physical level, algorithms for circuit cost optimization—specifically, due to combining decompositions of gates such as to enforce gate cancellations and single-qubit gate optimization, and physical-level designs of quantum logical gates and computational primitives. Our results help to bridge the gap between quantum computational experiments and a fully-fledged quantum

computer: indeed, our approach allows to automatically design and execute quantum algorithms on the existing hardware, which may be described as programming a quantum computer. We furthermore note that the techniques and circuit implementations developed are flexible enough to straightforwardly accommodate future anticipated changes in the controlling apparatus resulting in the changes to the circuit costing metrics.

7 Acknowledgements

Circuit diagrams were drawn using qcircuit.tex package, <http://physics.unm.edu/CQuIC/Qcircuit/>.

This material was based on work supported by the National Science Foundation, while working at the Foundation. Any opinion, finding, and conclusions or recommendations expressed in this material are those of the author and do not necessarily reflect the views of the National Science Foundation.

References

- [1] R. Blatt and D. J. Wineland, “Entangled states of trapped atomic ions”, *Nature* **453**, 1008–1015, 2008.
- [2] A. Barenco, C. H. Bennett, R. Cleve, D. P. DiVincenzo, N. Margolus, P. Shor, T. Sleator, J. Smolin, and H. Weinfurter, “Elementary gates for quantum computation”, *Phys. Rev. A* **52**, 3457–3467, 1995, [quant-ph/9503016](#).
- [3] R. B. Griffiths and C.-S. Niu, “Semiclassical Fourier transform for quantum computation”, *Phys. Rev. Lett.* **76**, 3228–3231, 1996, [quant-ph/9511007](#).
- [4] L. K. Grover, “A fast quantum mechanical algorithm for database search”, *Proceedings of 28th Annual ACM Symposium on the Theory of Computing*, pages 212–219, May 1996, [quant-ph/9605043](#).
- [5] S. Debnath, N. M. Linke, C. Figgatt, K. A. Landsman, K. Wright, and C. Monroe, “Demonstration of a programmable quantum computer module”, 2016, [arXiv:1603.04512](#).
- [6] S. Debnath, N. M. Linke, C. Figgatt, K. A. Landsman, and C. Monroe, *personal communication*, October 15, 2015.
- [7] D. P. DiVincenzo, “The physical implementation of quantum computation”, *Fortschritte der Physik* **48**(9-11):771–783, 2000, [quant-ph/0002077](#).
- [8] M. H. Devoret and R. J. Schoelkopf, “Superconducting circuits for quantum information: an outlook”, *Science* **339**, 1169–1174, 2013.
- [9] T. D. Ladd, F. Jelezko, R. Laflamme, Y. Nakamura, C. Monroe, and J. L. O’Brien, “Quantum computers”, *Nature* **464**, 45–53, 2010, [arXiv:1009.2267](#).
- [10] D. Maslov, “Advantages of using relative-phase Toffoli gates with an application to multiple control Toffoli optimization”, *Phys. Rev. A* **93**, 022311, 2016, [arXiv:1508.03273](#).
- [11] D. Maslov, G. W. Dueck, and D. M. Miller, “Techniques for the synthesis of reversible Toffoli networks”, *ACM Trans. on Design Automation of Electronic Systems* **12**(4), article 42, 2007, [quant-ph/0607166](#).
- [12] D. Maslov, G. W. Dueck, D. M. Miller, and C. Negrevergne, “Quantum circuit simplification and level compaction”, *IEEE Trans. CAD* **27**(3):436–444, 2008, [quant-ph/0604001](#).

- [13] T. Monz, K. Kim, W. Hänsel, M. Riebe, A. Villar, P. Schindler, M. Chwalla, M. Hennrich, and R. Blatt, “Realization of the quantum Toffoli gate with trapped ions”, *Phys. Rev. Lett.* **102**, 040501, 2009, [arXiv:0804.0082](#).
- [14] V. Nebendahl, H. Häffner, and C. F. Roos, “Optimal control of entangling operations for trapped ion quantum computing”, *Phys. Rev. A* **79**, 012312, 2009, [arXiv:0809.1414](#).
- [15] M. A. Nielsen and I. L. Chuang, *Quantum Computation and Quantum Information*, Cambridge University Press, New York, 2000.
- [16] A. K. Prasad, V. V. Shende, I. L. Markov, J. P. Hayes, and K. N. Patel, “Data structures and algorithms for simplifying reversible circuits”, *ACM Journal on Emerging Technologies in Computing Systems* **2**(4):277–293, 2006.
- [17] M. Saeedi and I. L. Markov, “Synthesis and optimization of reversible circuits – a survey”, *ACM Computing Surveys* **45**(2), article 21, 2013, [arXiv:1110.2574](#).
- [18] V. V. Shende and I. L. Markov, “On the CNOT-cost of Toffoli gates”, *Quantum Information and Computation* **9**(5-6), 461–486, 2009, [arXiv:0803.2316](#).
- [19] A. Sørensen and K. Mølmer, “Quantum computation with ions in thermal motion”, *Phys. Rev. Lett.* **82**, 1971–1974, 1999, [quant-ph/9810039](#).
- [20] T. R. Tan, J. P. Gaebler, Y. Lin, Y. Wan, R. Bowler, D. Leibfried, and D. J. Wineland, “Multi-element logic gates for trapped-ion qubits”, *Nature* **528**, 380–383, 2015, [arXiv:1508.03392](#).